

# Two Tags in One Probe: Combining Fluorescence- and Biotin-based Detection of the Trypanosomal Cysteine Protease Rhodesain

Carina Lemke,<sup>[a]</sup> Adéla Jílková,<sup>[b]</sup> Dominic Ferber,<sup>[a]</sup> Annett Braune,<sup>[c]</sup> Anja On,<sup>[a]</sup> Patrick Johe,<sup>[d]</sup> Alena Zíková,<sup>[e]</sup> Tanja Schirmeister,<sup>[d]</sup> Michael Mareš,<sup>[b]</sup> Martin Horn,<sup>\*,[b]</sup> and Michael Gütschow<sup>\*,[a]</sup>

**Abstract:** Rhodesain is the major cysteine protease of the protozoan parasite *Trypanosoma brucei* and a therapeutic target for sleeping sickness, a fatal neglected tropical disease. We designed, synthesized and characterized a bimodal activity-based probe that binds to and inactivates rhodesain. This probe exhibited an irreversible mode of action and extraordinary potency for the target protease with a  $k_{\text{inac}}/K_i$  value of  $37,000 \text{ M}^{-1}\text{s}^{-1}$ . Two reporter tags, a fluorescent coumarin moiety and a biotin affinity label, were incorporated

into the probe and enabled highly sensitive detection of rhodesain in a complex proteome by in-gel fluorescence and on-blot chemiluminescence. Furthermore, the probe was employed for microseparation and quantification of rhodesain and for inhibitor screening using a competition assay. The developed bimodal rhodesain probe represents a new proteomic tool for studying *Trypanosoma* pathobiochemistry and antitrypanosomal drug discovery.

## Introduction

Cysteine proteases of the papain family are widely recognized as therapeutically relevant targets in a large number of diseases, not only for different types of cancer and (auto-)immune disorders, but also for viral and protozoal infections.<sup>[1]</sup> Human African trypanosomiasis (HAT), also known as sleeping sickness, is transmitted by the tsetse fly (*Glossina* spp.) to humans. This trypanosomal disease can be subdivided into two forms, the gambiense and rhodesiense HAT, both distributed in Sub-Saharan Africa. The latter, transmitted by *Trypanosoma brucei rhodesiense*, shows a rapid disease progression, while *T. b. gambiense* causes a chronic infection, both with a mortality rate close to 100% if untreated. Another subspecies, *T. b. brucei* is the causative agent of Nagana in cattle. The current therapy of rhodesiense HAT, employing injections of suramin in the

hemolymphatic stage and melarsoprol in the meningoencephalitic stage, is not satisfactory.<sup>[2]</sup>

Rhodesain, a papain-like cysteine protease of *Trypanosoma brucei* spp., also known as TbCatL (*T. brucei* cathepsin L), has been identified as a target enzyme for the development of inhibitors to combat acute and chronic infections. The lysosomal protease is activated by either inter- or intramolecular catalysis, preferably at low pH.<sup>[3]</sup> However, in contrast to related human cathepsins, rhodesain also shows activity up to pH 8.0, consistent with a possible function in the host's blood stream.<sup>[4]</sup> Rhodesain plays an irreplaceable role in the life cycle of *T. b. rhodesiense* by supplying it with nutrients and hiding it from the host immune system.<sup>[5,6]</sup>

Several types of covalent peptidomimetic inhibitors have been reported for trypanosomal papain-like cysteine proteases, equipped with different warheads,<sup>[7]</sup> ranging from reversible


[a] C. Lemke, D. Ferber, A. On, Prof. Dr. M. Gütschow  
Pharmaceutical Institute  
Department of Pharmaceutical & Medicinal Chemistry  
University of Bonn  
An der Immenburg 4, 53121 Bonn (Germany)  
E-mail: guetschow@uni-bonn.de


[b] Dr. A. Jílková, Dr. M. Mareš, Dr. M. Horn  
Institute of Organic Chemistry and Biochemistry  
Czech Academy of Sciences  
Flemingovo n. 2, 16610 Prague (Czech Republic)  
E-mail: martin.horn@uochb.cas.cz

[c] Dr. A. Braune  
Research Group Intestinal Microbiology  
German Institute of Human Nutrition Potsdam-Rehbruecke  
Arthur-Scheunert-Allee 114–116  
14558 Nuthetal (Germany)

[d] Dr. P. Johe, Prof. Dr. T. Schirmeister  
Institute of Pharmaceutical and Biomedical Sciences (IPBS)  
Johannes Gutenberg University of Mainz  
Staudingerweg 5  
55128 Mainz (Germany)

[e] Dr. A. Zíková  
Biology Centre CAS, Institute of Parasitology  
University of South Bohemia  
Faculty of Science  
Branišovská 1160/31, 37005 České Budějovice (Czech Republic)

 Supporting information for this article is available on the WWW under <https://doi.org/10.1002/chem.202201636>

 © 2022 The Authors. Chemistry - A European Journal published by Wiley-VCH GmbH. This is an open access article under the terms of the Creative Commons Attribution Non-Commercial NoDerivs License, which permits use and distribution in any medium, provided the original work is properly cited, the use is non-commercial and no modifications or adaptations are made.

carbanitrile inhibitors<sup>[8,9]</sup> to irreversible Michael acceptors, which include vinylic ketones,<sup>[10,11]</sup> sulfones,<sup>[12,13]</sup> acrylates,<sup>[14]</sup> and enoates.<sup>[15]</sup> Two well-established pan-cathepsin inhibitors, the epoxide E-64<sup>[10]</sup> and the vinyl sulfone K11777<sup>[13,16]</sup> act as potent rhodesain inhibitors.

The principles of activity-based and substrate-based profiling are well established for human cysteine proteases.<sup>[17,18]</sup> However, only few examples of activity-based probes (ABPs) for protozoal cysteine proteases are known.<sup>[19,20]</sup> High affinity, an irreversible mode of action and a moiety for biochemical read-out are prerequisites of ABPs. On the one hand, fluorescence labels have received broad attention. On the other hand, biotin, owing to its strong affinity for avidin and streptavidin, serves in different activity-based technologies.<sup>[21]</sup> To combine both features in a single compound, we conceptualized an ABP for rhodesain, which possesses two labels, i.e. a fluorophore and biotin. This type of ABP will allow for various applications, including in-gel fluorescence detection and on-blot visualization using a chemiluminescent biotin-streptavidin system, but also target isolation, identification, and quantification. In the course of an optimization process guided by biochemical parameters of protease inhibition, we aimed at developing a peptidic vinyl sulfone linked to a fluorescent coumarin tag, which in turn should be linearly connected to a biotin label. Hence, we designed a bi-functionalized coumarin as the key building block to assemble the envisaged rhodesain-targeting ABP. The suitability of the rhodesain ABP was assessed with in-gel and on-blot detection and HPLC-based quantification experiments. In particular, our ABP was successfully employed in a unique combination of biotin-based affinity purification

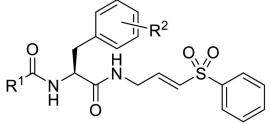
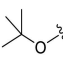
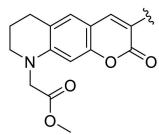
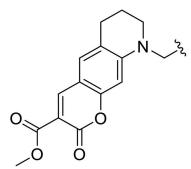
and size exclusion chromatography coupled to fluorescence detection.

## Results and Discussion

**Design and synthesis of precursors and probes guided by rhodesain inhibition kinetics.** In ABPs for cysteine proteases,  $\alpha,\beta$ -unsaturated Michael acceptors have already been installed as electrophilic warheads.<sup>[20]</sup> The nucleophilic attack of the active site cysteine thiolate at the  $\beta$ -carbon gives rise to covalent irreversible enzyme inhibition. The vinyl sulfone motif was advantageously implemented to assemble inhibitors of trypanosomal cysteine proteases<sup>[12,13]</sup> and therefore selected for the design of our activity-based probes. The structures of four ABPs (3–6) and two precursors (1, 2), all of which share the  $\alpha,\beta$ -unsaturated phenyl sulfone warhead are listed in Table 1. The compounds bear glycine at P1 and either 3-chlorophenylalanine or 4-methylphenylalanine at P2 position. We envisaged advantageous interactions of these P2 amino acid residues with the S2 pocket of rhodesain, based on previous studies.<sup>[9,22]</sup>

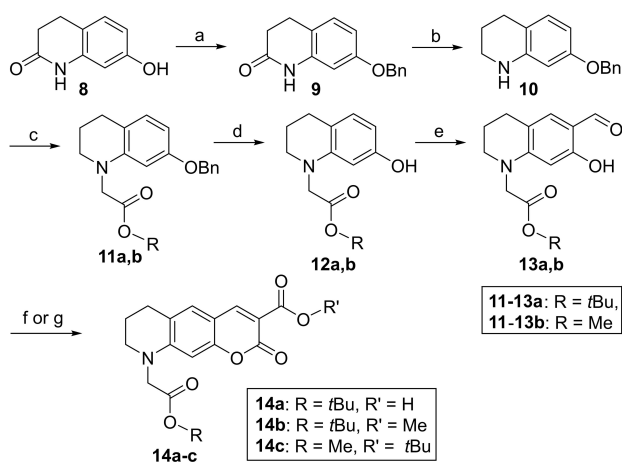
It was intended to implement an orthogonally addressable fluorescent moiety within the final activity-based probe. Coumarins are one group out of several fluorophores known to be incorporated as substrates or activity-based probes for protease activity investigations.<sup>[23]</sup> In addition, the fluorescence properties of coumarins benefit from large Stoke's shift, good quantum yield and the opportunity to fine-tune optical properties by tailored chemical modifications.<sup>[23]</sup> Rigidization of the 7-amino group due to cyclization improves fluorescence proper-

**Table 1.** Inhibition of rhodesain and human cathepsins by activity-based probes 3–7 and their precursors 1 and 2.

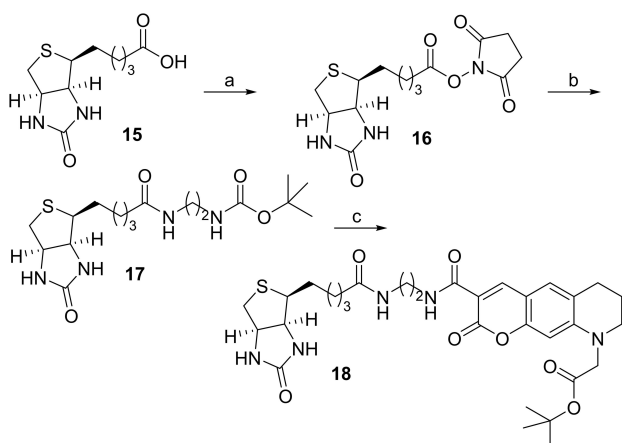
Compound	R <sup>1</sup>	R <sup>2</sup>			Rhodesain $k_{\text{inac}}/K_i$ (M <sup>-1</sup> s <sup>-1</sup> ) <sup>[a]</sup>	Cathepsin B	Cathepsin K	Cathepsin L	Cathepsin S
			Cathepsin B	Cathepsin K					
1		3-Cl	95,900	580	79% <sup>[c]</sup>	16,400	2,940		
2		4-CH <sub>3</sub>	139,000	161	n.i. <sup>[d]</sup>	5,840	3,640		
3		3-Cl	14,400	844	17% <sup>[c]</sup>	7,120	671		
4		4-CH <sub>3</sub>	1,510	53% <sup>[c]</sup>	40,800	52% <sup>[c]</sup>	527		
5		3-Cl	4,290	881	27,400	16,000	49,500		
6		4-CH <sub>3</sub>	16,100	391	n.i. <sup>[d]</sup>	12,000	5,510		
7 <sup>[b]</sup>			37,000	279	1,750	13,600	5,020		

[a] Second-order rate constant of protease inhibition, for further details, see Table S1. [b] For structure of ABP 7, see Scheme 3. [c] Percentage remaining enzymatic activity at 5  $\mu$ M inhibitor concentration. [d] n.i. = no inhibition (remaining activity at 5  $\mu$ M > 95 %).

ties and restores fluorescence in aqueous media. Herein, we took advantage of two different access points for functionalization and ultimate attachment of both biotin and the inhibitory structure on either side of a tricyclic aminocoumarin. For this purpose, we dissected one propylene chain from coumarin 343 to allow substitution at the coumarin's nitrogen. A linear, six-step route was employed for the synthesis of three different, orthogonally or mono-protected coumarin building blocks (Scheme 1). Hydroxyquinolinone **8** underwent etherification and borane-mediated reduction, followed by *N*-alkylation with either *tert*-butyl or methyl bromoacetate. Palladium-catalyzed hydrogenolysis re-established the free hydroxyl group, which, after Vilsmeier-Haack formylation and Knoevenagel condensation was utilized for lactonization. The obtained three coumarins **14a-c** were ready-to-use for incorporation in activity-based



**Scheme 1.** Synthetic route to coumarins **14a-c**. Reagents and conditions: (a) BnBr, K<sub>2</sub>CO<sub>3</sub>, DMF, rt, 16 h; (b) BH<sub>3</sub>×THF, THF, 0 °C to reflux, 2 h; (c) BrCH<sub>2</sub>CO<sub>2</sub>R (R = *t*Bu for **14a** and **14b**, R = Me for **14c**), K<sub>2</sub>CO<sub>3</sub>, DMF, 80 °C 16 h; (d) Pd/C, H<sub>2</sub>, MeOH, rt 3 h; (e) POCl<sub>3</sub>, DMF, 0 °C to rt, 1 h; (f) 2,2-dimethyl-1,3-dioxane-4,6-dione (for **14a**), piperidinium acetate, EtOH, rt to reflux, 2.5 h; (g) dimethyl malonate (for **14b**) or *tert*-butyl ethyl malonate (for **14c**), piperidine, toluene, reflux, 2 h.



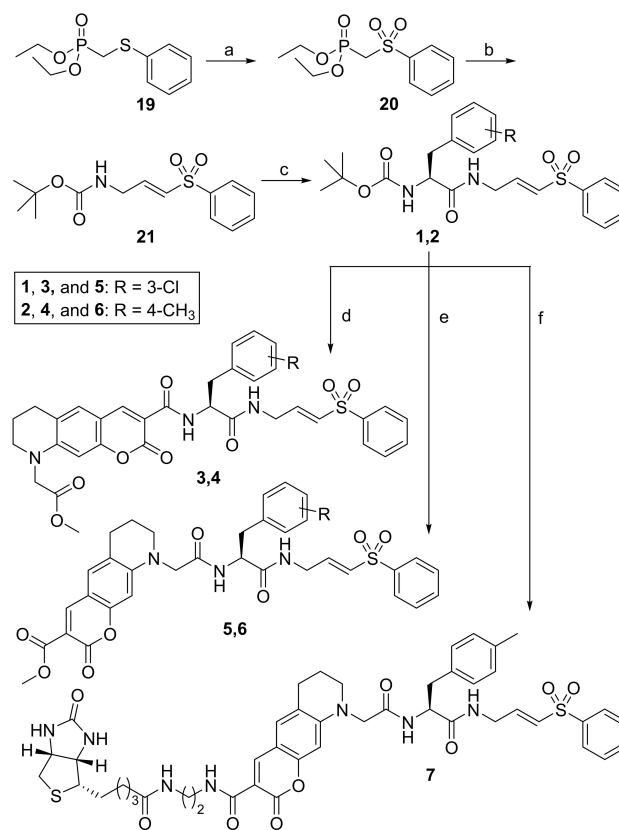
**Scheme 2.** Synthetic route to biotin-coumarin conjugate **18**. Reagents and conditions: (a) *N*-hydroxy succinimide, DCC, pyridine, DMF, 60 °C to rt, 16 h; (b) *N*-Boc-ethylene diamine, TEA, DMF, rt, 18 h; (c) (i) TFA, CH<sub>2</sub>Cl<sub>2</sub> (1 + 6), rt, 16 h, (ii) **14a**, HBTU, DIPEA, DMF, rt, 18 h.

probes. Absorption ( $\lambda_{\text{max}}$  420–426 nm) and emission spectra ( $\lambda_{\text{max}}$  468–470 nm) are shown in Figure S1.

As depicted in Scheme 2, a selected coumarin was connected with biotin. Activation of D-(+)-biotin (**15**), followed by coupling to mono-Boc-protected ethylenediamine,<sup>[24]</sup> and proton-catalyzed deprotection generated the biotin-linker building block **17**. The mono-protected coumarin derivative **14a** was employed in a uronium salt-mediated reaction to produce **18**.

Horner-Wadsworth-Emmons chemistry was applied for the warhead, which was connected to Boc-protected 3-chlorophenylalanine or 4-methylphenylalanine (Scheme 3) affording precursors **1** and **2**. In order to spot the preferred direction of the bifunctional coumarin, the lactone part was oriented towards the inhibitor substructure in ABPs **3** and **4**, and outward in ABPs **5** and **6**.

Precursors **1** and **2** and activity-based probes **3–6** were kinetically evaluated for their inhibitory efficacy towards the target protease rhodesain and the four related human cysteine cathepsins B, K, L, and S (Table 1). In in vitro assays with peptidic substrates, protease-catalyzed product formation was



**Scheme 3.** Synthetic route to inhibitors **1** and **2** and activity-based probes **3–7**. Reagents and conditions: (a) KMnO<sub>4</sub>, acetic acid/water (2 + 1), rt, 1.5 h; (b) Boc-Gly-H, KOTBu, THF, 0 °C to rt, 2 h; (c) (i) TFA, CH<sub>2</sub>Cl<sub>2</sub> (1 + 6), rt, 16 h, (ii) Boc-Phe(3-Cl)-OH or Boc-Phe(4-CH<sub>3</sub>)-OH, HBTU, DIPEA, CH<sub>2</sub>Cl<sub>2</sub>, rt, 18 h; (d) (i) **14c**, TFA, CH<sub>2</sub>Cl<sub>2</sub> (1 + 6), rt, 16 h, (ii) **1** or **2**, TFA, CH<sub>2</sub>Cl<sub>2</sub> (1 + 6), rt, 16 h, (iii) deprotected **14c**, deprotected **1** or **2**, HBTU, DIPEA, CH<sub>2</sub>Cl<sub>2</sub>, rt, 16 h; (e) **14b**, TFA, CH<sub>2</sub>Cl<sub>2</sub> (1 + 6), rt, 16 h, (ii) **1** or **2**, TFA, CH<sub>2</sub>Cl<sub>2</sub> (1 + 6), rt, 16 h, (iii) deprotected **14b**, deprotected **1** or **2**, HBTU, DIPEA, CH<sub>2</sub>Cl<sub>2</sub>, rt, 16 h; (f) **18**, TFA, CH<sub>2</sub>Cl<sub>2</sub> (1 + 4), rt, 3 h, (ii) **2**, TFA, CH<sub>2</sub>Cl<sub>2</sub> (1 + 6), rt, 16 h, (iii) deprotected **18**, deprotected **2**, HBTU, DIPEA, DMF, rt, 16 h.

monitored for 60 min. Typically, the compounds showed time-dependent inhibition with product formation rates approaching zero, indicating an irreversible binding mode. The inhibitory potency was quantified by the second-order rate constant  $k_{\text{inac}}/K_i$ . A benefit for rhodesain inhibition was deducible for the 4-methylphenylalanine in P2 position as realized in precursor **2**, rather than for the 3-chlorophenylalanine in **1**. Referring to target selectivity, **1** and **2** showed negligible or weak inhibition of cathepsins B, K and S. Compounds **1** and **2** affected cathepsin L, but still offered a good selectivity towards rhodesain with a selectivity ratio (SR rhodesain/cathepsin L) of 5.8 for **1** and 23.8 for **2**. The replacement of the Boc capping group (in **1** and **2**) by the coumarin with its lactone moiety oriented inward (in **3** and **4**) led to an inverse picture. Potency of both compounds dropped, and ABP **3** remained more active than **4** against rhodesain. In addition, the selectivity of **3** for rhodesain over cathepsin L was only 2-fold, while ABP **4** was unexpectedly even more active against cathepsin K than against rhodesain. Kinetic data of rhodesain inhibition by compounds **5** and **6** with the outward oriented lactone indicated the advantageous 4-methyl substitution of the P2 amino acid (in **6**), as already observed for precursor **2**, again reflecting a 'subsite cooperativity effect'. Among the four fluorescent ABPs **3**–**6**, the latter exhibited the strongest rhodesain inhibition, and although ABP **6** was not sufficiently selective (SR rhodesain/cathepsin L, 1.3; SR rhodesain/cathepsin S, 2.9), its structure was nominated for biotin incorporation. The desired ABP **7** was assembled from building blocks **14a**, **17** and **2** in a three-branched convergent synthesis. In the final step of this successfully accomplished preparation, precursor **2** was concomitantly deprotected and subjected to the final amide bond formation to give **7** (Scheme 3).

ABP **7** was kinetically characterized as an irreversible inhibitor of rhodesain (Figure 1). Gratifyingly, the ABP showed an impressively high second-order rate constant of inactivation,  $k_{\text{inac}}/K_i$  of  $37,000 \text{ M}^{-1}\text{s}^{-1}$  (Table 1). The two-fold improved inhibitory potency of ABP **7** in comparison to its fragment **6**

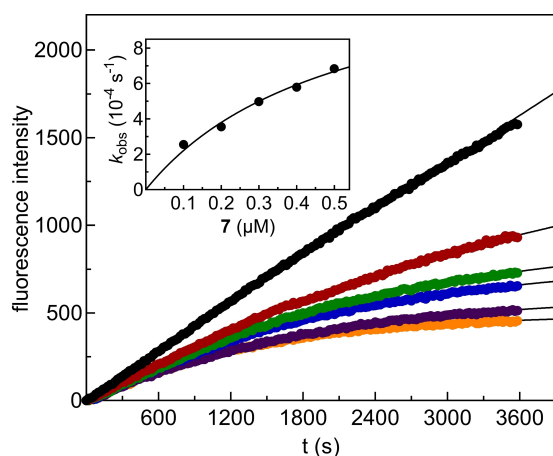


**Figure 1.** Inhibition of rhodesain by ABP **7**. The formation of 7-amino-4-methylcoumarin from the fluorogenic substrate Cbz-Phe-Arg-AMC was monitored ( $\lambda_{\text{ex}}$  360 nm,  $\lambda_{\text{em}}$  460 nm) at different inhibitor concentrations (from top to bottom: 0  $\mu\text{M}$ , 0.1  $\mu\text{M}$ , 0.2  $\mu\text{M}$ , 0.3  $\mu\text{M}$ , 0.4  $\mu\text{M}$ , and 0.5  $\mu\text{M}$ ).

indicated that the linker-connected biotin might contribute to the affinity for rhodesain. ABP **7** was selective for rhodesain over cathepsins B (SR 130) and K (SR 21), and exhibited a slight preference for rhodesain over cathepsins L (SR 2.7) and S (SR 7.4) (Table 1).

**Application of probe 7 for in-gel and on-blot imaging of rhodesain.** The favorable kinetic features of ABP **7** prompted us to evaluate it as a bimodal ABP for rhodesain imaging after gel electrophoresis (Figure 2). First, we examined the functionality of the fluorescent coumarin tag. Rhodesain was labeled with ABP **7**, subjected to SDS-PAGE and visualized by a fluorescence scanner, followed by Coomassie staining of proteins (Figure 3A). A fluorescent band at approximately 25 kDa corresponded to the rhodesain-**7** adduct; the signal was clearly diminished when rhodesain was treated with a mixture of the competitive inhibitors E-64 and K11777 prior to the labeling reaction. This finding corroborated the active-site directed mode of rhodesain inhibition by ABP **7**. In order to determine the detection limit, decreasing amounts of rhodesain were incubated with ABP **7**, resolved by SDS-PAGE and visualized by in-gel fluorescence imaging. Thus, rhodesain of as little as 100 ng was still visible (Figure 3A). Similar results were obtained for the non-biotin ABP **6** (Figure S2).

Next, we took advantage of the biotin label incorporated in ABP **7** for rhodesain on-blot imaging (Figure 2). The labeling experiments with SDS-PAGE separation were repeated, and the gels were electroblotted onto a PVDF membrane and visualized with the streptavidin-biotin chemiluminescent detection method (Figure 3B). Similar to the coumarin tag, imaging with the biotin label revealed a clear band of rhodesain, and labeling was specifically blocked upon rhodesain preincubation with competitive inhibitors. We detected a ten times lower amount of rhodesain (10 ng) compared to in-gel fluorescence. Both tags implemented in one single ABP **7** thus enabled efficient detection of active rhodesain, using two different imaging approaches. While the coumarin fluorescence permitted direct in-gel imaging, the biotin label allowed for more sensitive Western blot detection of the active target protease.

Furthermore, the selectivity of the ABP **7** was investigated in a complex protein mixture, namely the lysate of HEK cells not expressing rhodesain. A mixture of HEK cell lysate and rhodesain was treated with ABP **7**, resolved by SDS-PAGE, and

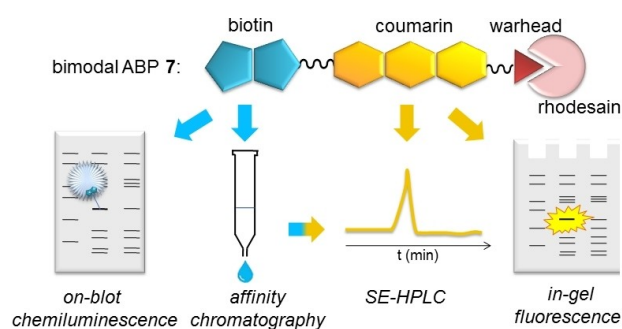


**Figure 2.** Schematic representation of the bimodal rhodesain ABP **7** and utilization of the two labels for various biochemical methods.

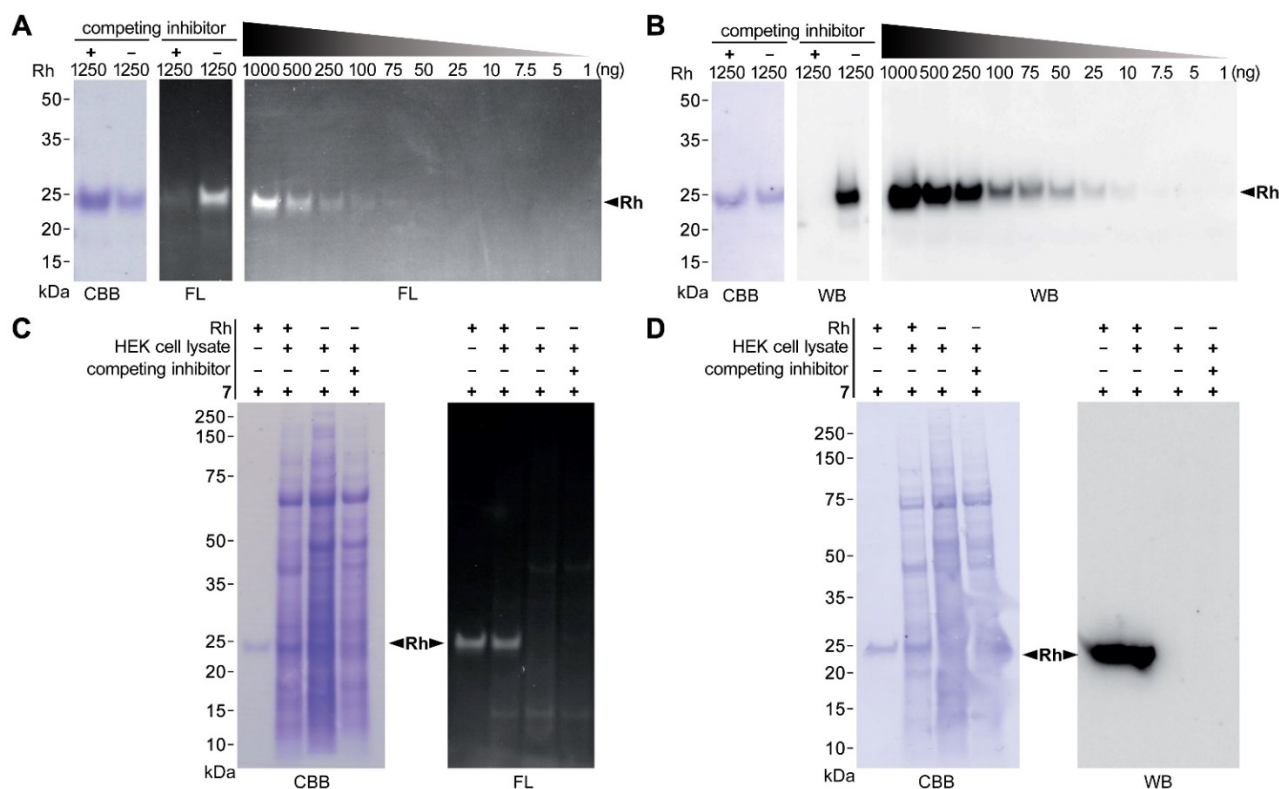


**Figure 3.** In-gel fluorescence (FL) and streptavidin-biotin Western blot chemiluminescence (WB) detection of rhodesain with ABP 7. (A, B) Purified recombinant rhodesain (Rh, 1–1250 ng) was incubated with ABP 7 (5  $\mu$ M) at 25  $^{\circ}$ C for 60 min. In a control experiment, rhodesain (1250 ng) was treated with a mixture of the competitive inhibitors E-64/K11777 (each 10  $\mu$ M) prior to incubation with ABP 7 (5  $\mu$ M). The samples were resolved by SDS-PAGE. (C, D) Rhodensain (Rh, 1250 ng), in the absence or presence of HEK cell lysate (30  $\mu$ g), was treated with ABP 7 (5  $\mu$ M) for 60 min at 25  $^{\circ}$ C. In a control experiment, HEK cell lysate (30  $\mu$ g), in the absence of rhodesain, was treated with ABP 7 (5  $\mu$ M). Also, HEK cell lysate (30  $\mu$ g) was pretreated with a mixture of the competitive inhibitors E-64/K11777 (each 10  $\mu$ M) prior to treatment with ABP 7 (5  $\mu$ M). The samples were resolved by SDS-PAGE. (A, C) In-gel detection was performed using a fluorescence scanner (FL) and the gels were subsequently stained with Coomassie Brilliant Blue (CBB). (B, D) For on-blot detection, the proteins were transferred on a PVDF membrane and visualized with the streptavidin-biotin Western blot chemiluminescence (WB) or stained with Coomassie Brilliant Blue (CBB).

visualized by fluorescence in-gel imaging employing the coumarin tag (Figure 3C), as well as by chemiluminescence on-blot detection using the biotin label (Figure 3D). In both cases, we detected a strong rhodesain band at approximately 25 kDa, as was observed for the labeling experiments in the absence of lysate. Treatment of only HEK cell lysate with ABP 7 did not result in any substantial signals despite the presence of excessive non-target proteins (Figure 3C, 3D), highlighting the superior selectivity of our probe. Unspecific weak fluorescence signals were not sensitive to pretreatment with a mixture of the competitive inhibitors E-64 and K11777, implying that they do not represent other catalytically active cysteine proteases (Figure 3C). Overall, these experiments with cell lysate indicated the usefulness of ABP 7 for rhodesain detection in complex protein mixtures.

**Application of probe 7 for visualization of rhodesain-like proteases in *T. brucei* cell lysates.** The functionality of ABP 7 was demonstrated by detecting native rhodesain-like proteases (TbCatLs) in the cell lysate of bloodstream forms of two *T. brucei* subspecies, *T. b. gambiense* and *T. b. brucei*. The TbCatLs from both of these parasites display more than 99% sequence identity to rhodesain from *T. b. rhodesiense*.<sup>[25]</sup> Labeling of

TbCatLs in the cell lysate was analyzed by in-gel fluorescence and on-blot chemiluminescence. For both subspecies studied, the ABP 7 labeled a major band of approximately 40 kDa (Figure 4) corresponding to the predicted molecular mass of the mature glycosylated TbCatL with its C-terminal domain.<sup>[4]</sup> The labeling signal was diminished when the cell lysate was pretreated with a mixture of the competitive inhibitors E-64 and K11777. The weaker bands at 30, 50 and 80 kDa observed with the chemiluminescent detection could represent different TbCatL forms with various glycosylation and proteolytic processing patterns. To determine the detection limit, decreasing amounts of lysate were incubated with ABP 7, resolved by SDS-PAGE, and visualized by both methods. The lowest protein content in the labeling reaction to detect the TbCatL signal was 50  $\mu$ g for in-gel and 10  $\mu$ g for on-blot visualization (Figure S3).

Furthermore, we exploited ABP 7 as a drug discovery tool for screening inhibitors of rhodesain and its homologs using a competition assay. First, the precursor inhibitors 1 and 2 were tested. They were preincubated at a wide concentration range with recombinant rhodesain or *T. b. brucei* cell lysate followed by labeling with ABP 7. The inhibitors blocked the target active site preventing the labeling and resulting in a suppressed

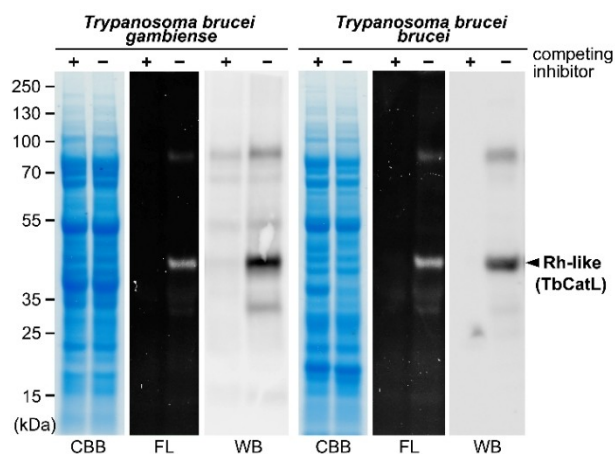


**Figure 4.** Imaging of rhodesain-like protease (TbCatL) in *T. brucei gambiense* and *T. brucei brucei* lysates with ABP 7. Cell lysates (80  $\mu$ g protein) were incubated with ABP 7 (5  $\mu$ M) at 25  $^{\circ}$ C for 60 min and resolved by SDS-PAGE. The gel was visualized using a fluorescence scanner (FL) and protein stained with Coomassie Brilliant Blue (CBB) or transferred onto a PVDF membrane and visualized with the streptavidin-biotin Western blot chemiluminescence (WB). In a control experiment, cell lysates were treated with a mixture of the competitive inhibitors E-64/K11777 (each 10  $\mu$ M) prior to incubation with ABP 7.

signal. Significantly lowered signals were observed at concentrations of 400 nM for labeling of rhodesain (Figure 5A) and 80 nM for labeling of cell lysate (Figure 5B). Second, the competition assay with rhodesain was used to screen a set of peptidomimetic inhibitors with vinyl sulfone warheads (Fig-

ure S4), known to be active against trypanosomal cysteine proteases.<sup>[4,26]</sup> These inhibitors reduced the rhodesain signal with various efficiencies, indicating differences in their inhibitory potency (Figure 5C).

To summarize, our results demonstrated that ABP 7 can be employed for labeling of rhodesain-type proteases in *Trypanosoma* proteomes and for competition profiling strategies to identify selective rhodesain inhibitors.

**Size-exclusion (SE) chromatography for the detection of fluorescently labeled rhodesain.** SE-HPLC constitutes an established technique for purification and identification of proteins. Concomitant UV and fluorescence detection has already been used for the characterization of an active protease, i.e. the serine protease matriptase,<sup>[27]</sup> and was employed for this study as well (Figure 2). After validation of the chromatographic system using standard proteins (Figure S5), varying amounts of rhodesain were incubated with ABP 7 for quantification (Figure 6A) in the presence of bovine serum albumin (BSA) to avoid rhodesain autoproteolysis. Aliquots were applied to the column, and chromatograms were analyzed with respect to the areas under the curve (AUCs) obtained by fluorescence detection, which referred to the peak of the rhodesain-7 adduct. The AUCs were linearly proportional to the applied rhodesain concentrations ranging from 10 to 80  $\mu$ g/mL (Figure 6A). In an analogous manner, SE-HPLC-based quantification of rhodesain with the non-biotin ABP 6 was conducted (Figure S6).

Subsequently, the SE-HPLC-based detection of rhodesain was investigated in the complex protein mixture of a HEK cell lysate. Following incubation with ABP 7, the rhodesain-supplemented lysate was analyzed by SE-HPLC with

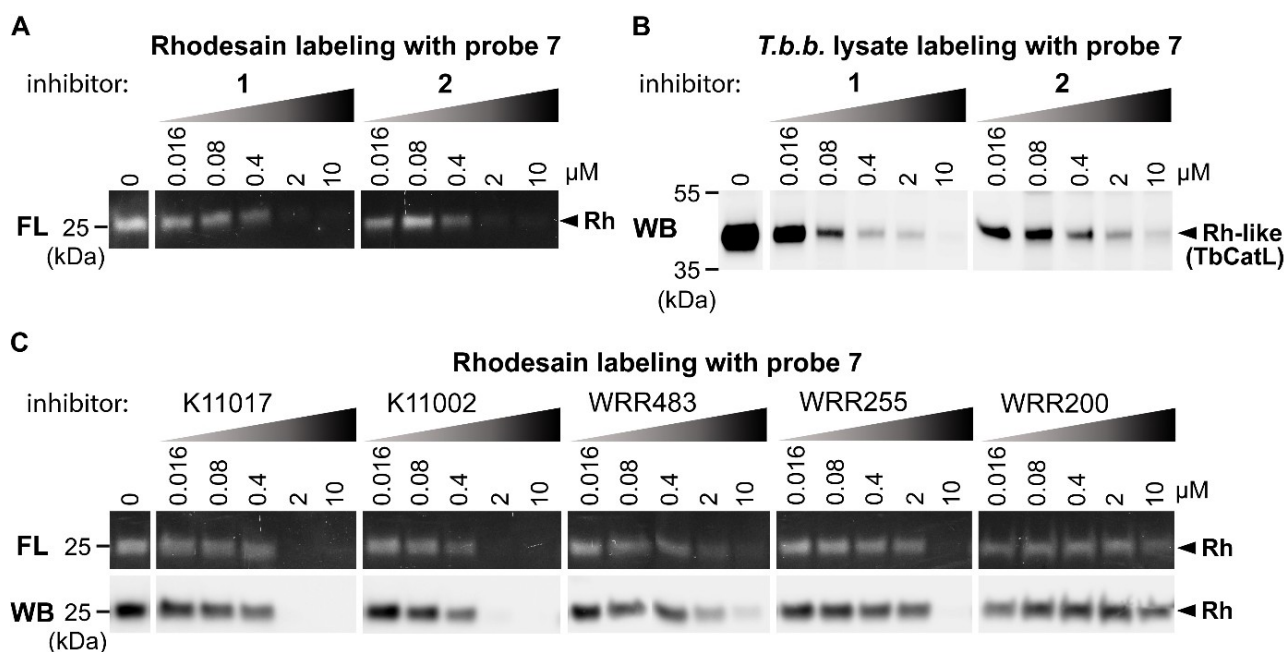


**Figure 5.** Competition profiling assay with ABP 7 and a set of rhodesain inhibitors. (A) Recombinant rhodesain (1  $\mu$ g) or (B) *T. b. brucei* cell lysate (80  $\mu$ g protein) were pretreated with the parent inhibitors 1 and 2 (0.016–10  $\mu$ M) at 37  $^{\circ}$ C for 15 min and then labeled with ABP 7 (5  $\mu$ M) at 25  $^{\circ}$ C for 60 min. (C) Recombinant rhodesain (1  $\mu$ g) was pretreated with five reactive peptidomimetic inhibitors of trypanosomal cysteine proteases (0.016–10  $\mu$ M) at 37  $^{\circ}$ C for 15 min and then labeled with ABP 7 (5  $\mu$ M) at 25  $^{\circ}$ C for 60 min. The reactions were resolved by SDS-PAGE and the gels were visualized using a fluorescence scanner (FL) or transferred onto a PVDF membrane and visualized with the streptavidin-biotin Western blot chemiluminescence (WB).

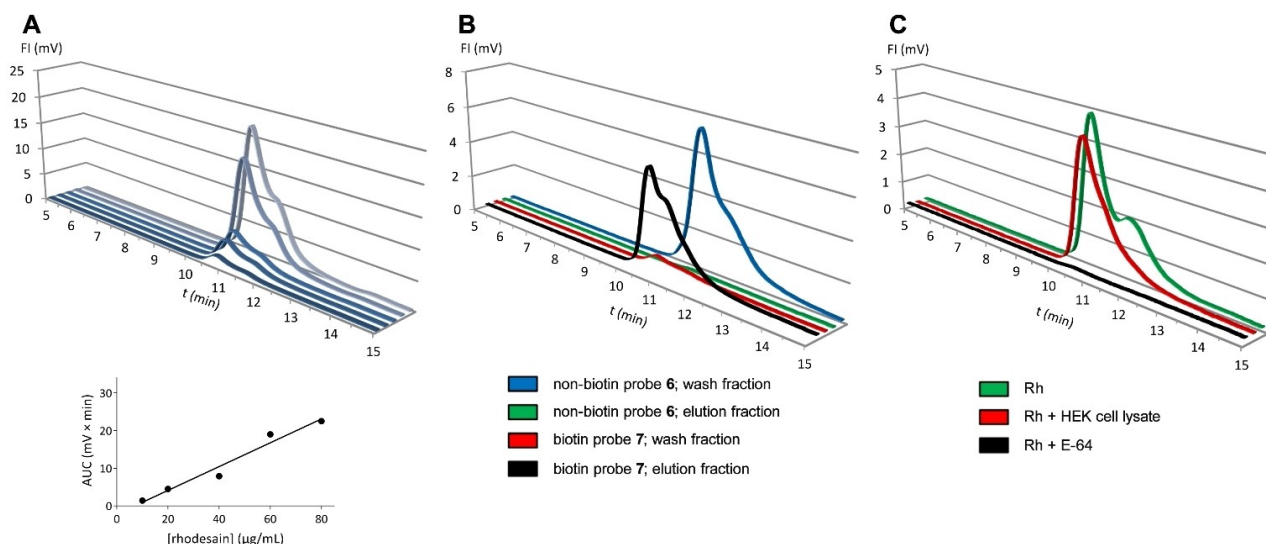


**Figure 6.** Application of the rhodesain probes using SE-HPLC with fluorescence detection. (A) Quantification of rhodesain with ABP 7 by SE-HPLC with fluorescence detection. Rhodensain at increasing concentrations (10–80 µg/mL) was incubated with BSA (0.5 µg) and ABP 7 (15 µM) for 60 min at 25 °C and pH 5.5. Protein was precipitated, resuspended, subjected to SE-HPLC and detected by fluorescence ( $\lambda_{\text{ex}} = 426$  nm;  $\lambda_{\text{em}} = 470$  nm; gain = 10; FI = fluorescence intensity). Chromatograms of a representative experiment are depicted. The diagram shows the correlation of areas under the curve (AUCs) and rhodensain concentrations ( $n = 3$ ). Linear regression gave  $y = 0.32x - 2.2$ . (B) SE-HPLC with fluorescence detection of rhodensain labeled with ABP 6 or 7 in wash and elution fractions from streptavidin affinity chromatography. Rhodensain (2 µg) was incubated with BSA (0.5 µg) and 15 µM of ABP 7 (black and red lines) or ABP 6 (green and blue lines) for 60 min at 25 °C and pH 5.5. After affinity chromatography using Strep-Tactin XT columns, the elution fractions (black and green lines) and wash fractions (red and blue lines) were concentrated and subjected to SE-HPLC analysis with fluorescence detection ( $\lambda_{\text{ex}} = 426$  nm;  $\lambda_{\text{em}} = 470$  nm; gain = 10; FI = fluorescence intensity). (C) SE-HPLC with fluorescence detection of elution fractions from streptavidin affinity chromatography of rhodensain (Rh) labeled with ABP 7 in the presence or absence of HEK cell lysate or competitor E-64. Rhodensain (2 µg) was incubated with BSA (0.5 µg) and ABP 7 (15 µM) for 60 min at 25 °C and pH 5.5 in the absence (green line) and presence of HEK cell lysate (45 µg) (red line). Additionally, a mixture of rhodensain and BSA was preincubated with E-64 (15 µM) at 37 °C for 15 min, followed by treatment with ABP 7 (black line). After affinity chromatography using Strep-Tactin XT columns, the elution fractions were concentrated and subjected to SE-HPLC analysis with fluorescence detection ( $\lambda_{\text{ex}} = 426$  nm;  $\lambda_{\text{em}} = 470$  nm; gain = 10; FI = fluorescence intensity).

fluorescence detection (Figure S7) and similar chromatograms were obtained for rhodensain in the presence or absence of HEK cell lysate. This result indicated the preferred reaction of ABP 7 with rhodensain rather than with the predominant non-target proteins. The generation of the fluorescent rhodensain-7 adduct was completely abolished by adding the irreversible cysteine protease inhibitor E-64. These data were in line with those obtained from the in-gel fluorescence imaging experiments (Figure 3A, 3C). The non-biotin ABP 6 was also utilizable for rhodensain detection in the presence of lysate (Figure S8). Excess of non-target proteins was demonstrated by UV monitoring of SE-HPLC (Figure S9). Overall, we demonstrated SE-HPLC with fluorescence detection to be appropriate for the detection of a cysteine protease, i.e. rhodensain, using ABPs.

**Affinity chromatography followed by SE-HPLC to detect labeled rhodensain.** The following set of experiments made simultaneous use of the two labels conferred by ABP 7 to the target protein rhodensain. We exploited activity-based probing through a combination of affinity chromatography and SE-HPLC for target purification and fluorescence-based quantification, respectively (Figure 2). Rhodensain was treated with ABP 7 and captured on a streptavidin affinity column. It was washed and rhodensain was eluted with buffer containing 50 mM biotin. The wash and elution fractions were each subjected to subsequent centrifugal concentration and buffer exchange to remove excess biotin from the elution fraction. We obtained an elution

and a wash fraction of ca. 60 µL each and used 20 µL thereof for HPLC separation. The resulting chromatograms (Figure 6B) revealed the fluorescently labeled rhodensain mainly in the elution fraction. Rhodensain was quantified according to the linear regression of the AUC versus concentration plot (Figure 6A). An approximately 75% recovery of the initially applied rhodensain was achieved in the elution fraction, while the wash fraction contained only a minor amount of the rhodensain-7 adduct (Figure 6B). On the contrary, when the same experimental setting was employed with the non-biotin ABP 6, the fluorescently labeled protease was completely recovered in the wash fraction and absent in the elution fraction (Figure 6B). These data highlighted the value of ABP 7 for rhodensain recovery by means of affinity chromatography and displayed by SE-HPLC.

Next, affinity chromatography was used for purification of labeled rhodensain from a complex protein mixture of HEK cell lysate and subsequent SE-HPLC target analysis was performed. For this purpose, ABP 7 was added to mixtures of rhodensain and HEK cell lysate, or rhodensain and E-64, or rhodensain alone. Non-target proteins were removed by streptavidin affinity chromatography and elution fractions of these incubations were analyzed by SE-HPLC with fluorescence detection (Figure 6C). Pretreatment with E-64 prevented rhodensain labeling and its occurrence in the elution fraction. We observed similar AUCs in chromatograms from incubations of rhodensain with

and without HEK cell lysate, although peak shapes differed. Without lysate, a peak shoulder at longer retention time most likely resulted from partial proteolysis of the rhodesain-7 adduct catalyzed by not yet labeled rhodesain. With HEK cell lysate, approximately 70% of rhodesain was recovered. These results demonstrate the utility of the bimodal ABP **7**, which allowed the combination of two sequential bioanalytical procedures to separate and quantify rhodesain (Figure 2).

## Conclusions

In this study, we developed a tailored ABP (**7**) for the detection of the cysteine protease rhodesain from *Trypanosoma brucei*, a therapeutically relevant target for the treatment of sleeping sickness. ABP **7** was equipped with two linearly arranged labels, both of which enabled sensitive rhodesain detection following SDS-PAGE. In particular, the biotin-based chemiluminescence measurements provided a low on-blot detection limit. Specificity of rhodesain detection was demonstrated in complex protein mixtures. Post-labeling quantification of active rhodesain was accomplished by means of SE-HPLC with coumarin fluorescence monitoring. The probe-mediated biotinylation of rhodesain was exploited for affinity purification of the target protein with satisfactory recovery as shown by subsequent SE-HPLC quantification employing fluorescence detection. The bimodal ABP can serve as a valuable tool for further bioanalytical approaches combining affinity chromatography with in-gel or on-blot detection of rhodesain to study *Trypanosoma* pathobiochemistry. Our probe was demonstrated to be suitable for drug screening to assess the interaction of rhodesain with potential inhibitors in competition assays in a cellular environment. Moreover, the modular concept by which the probe was developed can be modified and beneficially repurposed for targeting other proteases.

## Experimental Section

**Chemistry:** Materials, general chemical methods and detailed descriptions of synthetic procedures as well as analytical properties of all prepared compounds are given in the Supporting Information. Preparations and analytical data of compounds **14a**, **18**, and **7** are noted below.

**Compound 14a:** *tert*-Butyl 2-(6-formyl-7-hydroxy-3,4-dihydroquinolin-1(2*H*)-yl)acetate (**13a**, 0.38 g, 1.30 mmol) was dissolved in absolute ethanol (15 mL). Piperidinium acetate (4 mg, 0.03 mmol) and 2,2-dimethyl-1,3-dioxane-4,6-dione (0.19 g, 1.30 mmol) were added and the reaction was stirred at room temperature for 30 min. Then, the reaction was refluxed for further 2 h. Cooling to room temperature and subsequent cooling on ice led to the crystallization of **14a** as a bright yellow solid (0.21 g, 0.60 mmol, 46%, m.p. = 196–198 °C). <sup>1</sup>H NMR (600 MHz, DMSO-*d*<sub>6</sub>) δ 1.41 (s, 9H, C(CH<sub>3</sub>)<sub>3</sub>), 1.87 (p, <sup>3</sup>J = 6.4 Hz, 2H, NCH<sub>2</sub>CH<sub>2</sub>CH<sub>2</sub>), 2.72 (t, <sup>3</sup>J = 6.2 Hz, 2H, N(CH<sub>2</sub>)<sub>2</sub>CH<sub>2</sub>), 3.39–3.42 (m, 2H, NCH<sub>2</sub>(CH<sub>2</sub>)<sub>2</sub>), 4.21 (s, 2H, NCH<sub>2</sub>CO), 6.37 (s, 1H, 10-H), 7.38 (s, 1H, 5-H), 8.51 (s, 1H, 4-H), 12.51 (s, 1H, CO<sub>2</sub>H); <sup>13</sup>C NMR (150 MHz, DMSO-*d*<sub>6</sub>) δ 20.89 (NCH<sub>2</sub>CH<sub>2</sub>CH<sub>2</sub>), 26.83 (N(CH<sub>2</sub>)<sub>2</sub>CH<sub>2</sub>), 27.88 (C(CH<sub>3</sub>)<sub>3</sub>), 50.16 (NCH<sub>2</sub>(CH<sub>2</sub>)<sub>2</sub>), 53.25 (NCH<sub>2</sub>CO), 81.55 (C(CH<sub>3</sub>)<sub>3</sub>), 95.69 (C-10), 108.06, 108.14 (C-3, C-4a), 121.02, 129.56, 149.33, 151.53 (C-4, C-5, C-5a, C-9a), 156.60 (C-10a), 159.59

(C-2), 164.59, 168.45 (OCOC(CH<sub>3</sub>)<sub>3</sub>, CO<sub>2</sub>H); LC/MS (ESI) m/z: 360.0 [M + H]<sup>+</sup>, 99% purity.

**Compound 18:** *tert*-Butyl (2-(5-((3*a*,5*a*,6*a*)-2-oxohexahydro-1*H*-thieno[3,4-*d*]imidazol-4-yl)pentanamido)ethyl)carbamate (**17**, 0.18 g, 0.47 mmol) was suspended in dry CH<sub>2</sub>Cl<sub>2</sub> (12 mL) and stirred on ice. TFA (2 mL) was added and the reaction was stirred at room temperature for 16 h. The solvent was evaporated under reduced pressure and remaining TFA was removed with dry CH<sub>2</sub>Cl<sub>2</sub> (3 × 5 mL). The crude was used without further purification (0.19 g, 0.47 mmol, > 99%). Completion of the reaction was proven by TLC (CH<sub>2</sub>Cl<sub>2</sub>/MeOH 9 + 1). 9-(2-(*tert*-Butoxy)-2-oxoethyl)-2-oxo-6,7,8,9-tetrahydro-2*H*-pyrano[3,2-*g*]quinoline-3-carboxylic acid (**14a**, 0.17 g, 0.47 mmol), HBTU (0.27 g, 0.71 mmol) and DIPEA (0.10 mL, 0.59 mmol, 76 mg) were dissolved in DMF (15 mL) and stirred at room temperature under argon for 30 min. The deprotected TFA salt of **17** (0.19 g, 0.47 mmol) and DIPEA (0.10 mL, 0.59 mmol, 76 mg) dissolved in DMF (5 mL) were added dropwise to the reaction mixture, which was stirred at room temperature under argon for further 18 h. Purification using column chromatography with CH<sub>2</sub>Cl<sub>2</sub>/MeOH 9 + 1 as eluent yielded **18** as a yellow solid (0.15 g, 0.24 mmol, 52%, m.p. = 218–220 °C, under decomposition). <sup>1</sup>H NMR (600 MHz, DMSO-*d*<sub>6</sub>) δ 1.38–1.44 (m, 11H, C(CH<sub>3</sub>)<sub>3</sub>, CO-(CH<sub>2</sub>)<sub>2</sub>CH<sub>2</sub>), 1.46–1.52 (m, 3H, COCH<sub>2</sub>CH<sub>2</sub>CH<sub>2</sub>, CH<sub>2</sub>CHS), 1.55–1.62 (m, 1H, CH<sub>2</sub>CHS), 1.87 (p, <sup>3</sup>J = 5.9 Hz, 2H, NCH<sub>2</sub>CH<sub>2</sub>CH<sub>2</sub>), 2.04 (t, <sup>3</sup>J = 7.2 Hz, 2H, COCH<sub>2</sub>(CH<sub>2</sub>)<sub>2</sub>), 2.54 (d, <sup>2</sup>J = 12.4 Hz, 1H, SCH<sub>2</sub>), 2.71–2.78 (m, 3H, SCH<sub>2</sub>, N(CH<sub>2</sub>)<sub>2</sub>CH<sub>2</sub>), 3.01–3.07 (m, 1H, SCH), 3.19 (q, <sup>3</sup>J = 6.1 Hz, 2H, NH(CH<sub>2</sub>)<sub>2</sub>NH), 3.35 (q, <sup>3</sup>J = 6.2 Hz, 2H, NH(CH<sub>2</sub>)<sub>2</sub>NH), 3.40 (t, <sup>3</sup>J = 5.7 Hz, 2H, NCH<sub>2</sub>(CH<sub>2</sub>)<sub>2</sub>), 4.08 (dt, <sup>3</sup>J = 5.7 Hz, <sup>4</sup>J = 2.9 Hz, 1H, NHCH), 4.20 (s, 2H, NCH<sub>2</sub>CO), 4.23–4.29 (m, 1H, NHCH), 6.31 (s, 1H, NHCONH), 6.38 (s, 1H, NHCONH), 6.42 (s, 1H, 10-H), 7.43 (s, 1H, 5-H), 7.89 (t, <sup>3</sup>J = 5.6 Hz, 1H, CH<sub>2</sub>CONH), 8.59 (s, 1H, 4-H), 8.67 (t, <sup>3</sup>J = 5.8 Hz, 1H, CH<sub>2</sub>CONH); <sup>13</sup>C NMR (150 MHz, DMSO-*d*<sub>6</sub>) δ 20.93 (NCH<sub>2</sub>CH<sub>2</sub>CH<sub>2</sub>), 25.42 (CH<sub>2</sub>CHS), 26.90 (N(CH<sub>2</sub>)<sub>2</sub>CH<sub>2</sub>), 27.92 (C(CH<sub>3</sub>)<sub>3</sub>), 28.18, 28.28 (COCH<sub>2</sub>(CH<sub>2</sub>)<sub>2</sub>), 35.39, 38.46, 38.87 (NH(CH<sub>2</sub>)<sub>2</sub>NH, COCH<sub>2</sub>(CH<sub>2</sub>)<sub>2</sub>), 50.10 (NCH<sub>2</sub>(CH<sub>2</sub>)<sub>2</sub>), 53.23 (NCH<sub>2</sub>CO), 55.53 (SCH), 59.35, 61.13 (NHCH), 81.51 (C(CH<sub>3</sub>)<sub>3</sub>), 95.62 (C-10), 108.35, 110.27 (C-3, C-4a), 121.15, 129.40, 147.62, 151.04 (C-4, C-5, C-5a, C-9a), 155.90 (C-10a), 161.65, 162.53, 162.83 (C-2, NHCONH, CONH), 168.55, 172.46 (OCOC(CH<sub>3</sub>)<sub>3</sub>, CONH); the carbon signal for SCH<sub>2</sub> is obscured by the DMSO solvent signal. LC/MS (ESI) m/z: 628.5 [M + H]<sup>+</sup>, 98% purity.

**Compound 7:** (*S,E*)-*tert*-Butyl 1-oxo-1-(3-(phenylsulfonyl)allylamino)-3-*p*-tolylpropan-2-ylcarbamate (**2**, 92 mg, 0.20 mmol) was dissolved in dry CH<sub>2</sub>Cl<sub>2</sub> (6 mL) and stirred on ice. TFA (1 mL) was added and the reaction was stirred at room temperature for 16 h. The solvent was evaporated under reduced pressure and remaining TFA was removed with dry CH<sub>2</sub>Cl<sub>2</sub> (3 × 5 mL). The crude was used without further purification. The *tert*-butyl ester of protected compound **17** (0.13 g, 0.20 mmol) was cleaved in an analogous manner. The crude was used without further purification. Completion of both aforementioned reactions was proven by TLC. Deprotected **17** (0.20 mmol, 0.11 g), HBTU (0.30 mmol, 0.11 g), and DIPEA (43 μL, 0.25 mmol, 33 mg) were dissolved in DMF (15 mL) and stirred at room temperature under argon for 30 min. The TFA salt of deprotected **2** (95 mg, 0.20 mmol) and DIPEA (43 μL, 0.25 mmol, 33 mg) dissolved in DMF (5 mL) were added dropwise to the reaction mixture, which was stirred at room temperature under argon for further 18 h. The solvent was removed under reduced pressure and the crude residue was purified using column chromatography with CH<sub>2</sub>Cl<sub>2</sub>/MeOH 9 + 1 yielding **7** as a yellow solid (0.11 g, 0.12 mmol, 60%, m.p. = 158–160 °C). <sup>1</sup>H NMR (600 MHz, DMSO-*d*<sub>6</sub>) δ 1.39–1.53 (m, 5H) and 1.56–1.61 (m, 1H, CO(CH<sub>2</sub>)<sub>2</sub>CH<sub>2</sub>, COCH<sub>2</sub>CH<sub>2</sub>CH<sub>2</sub>, CH<sub>2</sub>CHS), 1.80–1.84 (m, 2H, NCH<sub>2</sub>CH<sub>2</sub>CH<sub>2</sub>), 2.05 (t, <sup>3</sup>J = 7.2 Hz, 2H, COCH<sub>2</sub>(CH<sub>2</sub>)<sub>2</sub>), 2.19 (s, 3H, 4-CH<sub>3</sub>), 2.54 (d, <sup>2</sup>J = 12.5 Hz, 1H, SCH<sub>2</sub>), 2.70 (t, <sup>3</sup>J = 6.3 Hz, 2H, N(CH<sub>2</sub>)<sub>2</sub>CH<sub>2</sub>), 2.74–2.77 (m, 2H, SCH<sub>2</sub>,



CHCH<sub>2</sub>Phe(4-CH<sub>3</sub>), 2.95 (dd, <sup>2</sup>J = 13.8 Hz, <sup>3</sup>J = 5.2 Hz, 1H, CHCH<sub>2</sub>Phe(4-CH<sub>3</sub>), 3.01–3.07 (m, 1H, SCH), 3.20 (q, <sup>3</sup>J = 6.2 Hz, 2H, NH(CH<sub>2</sub>)<sub>2</sub>NH), 3.33–3.39 (m, 4H, NH(CH<sub>2</sub>)<sub>2</sub>NH, NCH<sub>2</sub>(CH<sub>2</sub>)<sub>2</sub>), 3.91–4.01 (m, 3H, NHCH<sub>2</sub>Phe(4-CH<sub>3</sub>), NHCH<sub>2</sub>CH, NCH<sub>2</sub>CO), 4.04–4.10 (m, 2H, NHCH<sub>2</sub>biotin, NCH<sub>2</sub>CO), 4.25 (dd, <sup>3</sup>J = 7.7 Hz, <sup>3</sup>J = 5.0 Hz, 1H, NHCH<sub>2</sub>biotin), 4.45 (td, <sup>3</sup>J = 8.5 Hz, <sup>3</sup>J = 5.3 Hz, 1H, NHCH<sub>2</sub>CH), 6.29 (s, 1H, 10-H), 6.31 (s, 1H, NHCONH), 6.38 (s, 1H, NHCONH), 6.59 (dt, <sup>3</sup>J = 15.2 Hz, <sup>4</sup>J = 1.9 Hz, 1H, CHCHSO<sub>2</sub>), 6.83 (dt, <sup>3</sup>J = 15.1 Hz, <sup>3</sup>J = 4.3 Hz, 1H, CHCHSO<sub>2</sub>), 7.00–7.06 (m, 4H, 2'-H, 3'-H), 7.39 (s, 1H, 5-H), 7.62 (t, <sup>3</sup>J = 7.8 Hz, 2H, 3''-H), 7.69–7.73 (m, 1H, 4''-H), 7.80–7.82 (m, 2H, 2''-H), 7.85–7.91 (m, 1H, CONH), 8.29 (d, <sup>3</sup>J = 8.1 Hz, 1H, CONH), 8.36 (t, <sup>3</sup>J = 5.8 Hz, 1H, CONH), 8.58 (s, 1H, 4-H), 8.71 (t, <sup>3</sup>J = 5.9 Hz, 1H, CONH); <sup>13</sup>C NMR (150 MHz, DMSO-d<sub>6</sub>) δ 20.77 (NCH<sub>2</sub>CH<sub>2</sub>CH<sub>2</sub>), 20.85 (4-CH<sub>3</sub>), 25.42 (CH<sub>2</sub>CH<sub>2</sub>S), 26.88 (N(CH<sub>2</sub>)<sub>2</sub>CH<sub>2</sub>), 28.18, 28.29 (COCH<sub>2</sub>(CH<sub>2</sub>)<sub>2</sub>), 35.40 (NH(CH<sub>2</sub>)<sub>2</sub>NH), 37.20 (CHCH<sub>2</sub>Phe(4-CH<sub>3</sub>)), 38.50, 38.85 (NH(CH<sub>2</sub>)<sub>2</sub>NH and SCH<sub>2</sub> or COCH<sub>2</sub>CH<sub>2</sub>), 39.07 (NHCH<sub>2</sub>CH), 50.40 (NCH<sub>2</sub>(CH<sub>2</sub>)<sub>2</sub>), 53.68, (NCH<sub>2</sub>CO), 54.37 (NHCH<sub>2</sub>Phe(4-CH<sub>3</sub>)), 55.52 (SCH), 59.35, 61.14 (NHCH<sub>2</sub>biotin), 95.55 (C-10), 108.16, 109.79 (C-3, C-4a), 121.09 (C-4 or C-5 or C-5a or C-9a), 127.21 (C-2'' or C-3''), 128.87 (C-2'), 129.05 (C-3'), 129.20 (C-4'), 129.73 (C-2'' or C-3''), 129.94 (C-4 or C-5 or C-5a or C-9a), 133.79 (CHCHSO<sub>2</sub>), 134.48 (C-1' or C-4'), 135.43 (C-1' or C-4'), 140.50 (CHCHSO<sub>2</sub>), 144.35 (C-1''), 147.57, 151.20 (C-4 or C-5 or C-5a or C-9a), 155.99 (C-10a), 161.72, 162.63, 162.85 (NHCONH, C-2, CONH), 168.12, 171.14, 172.45 (CONH). The carbon signal for either SCH<sub>2</sub> or COCH<sub>2</sub>CH<sub>2</sub> is obscured by the DMSO solvent signal. LC/MS (ESI) m/z: 912.4 [M + H]<sup>+</sup>, 95% purity.

**Biology:** The zymogen of *T. b. rhodesiense* rhodesain (Uniprot Q95PM0) was heterologously expressed without its C-terminal domain in *Pichia pastoris* as described elsewhere.<sup>[3,4]</sup> Autoactivated rhodesain from the *Pichia* culture supernatants was purified on a phenyl sepharose column. Concentrated rhodesain solutions were lyophilized and stored at –80 °C. Stock solutions of ABPs and inhibitors were prepared in DMSO. Cathepsin inhibition assays<sup>[28,29]</sup> are described in the Supporting Information.

**General enzymatic methods:** Spectrophotometric assays (405 nm) were performed in cuvettes on a Varian Cary 50 Bio or 100 Bio device (Agilent). Fluorometric assays (λ<sub>ex</sub> = 360 nm, λ<sub>em</sub> = 460 nm) were performed on a FLUOstar Optima plate reader (BMG Labtech) in 96-well plates. Human cathepsin B was purchased from Calbiochem, human cathepsins K, L, and S were purchased from Enzo Life Sciences. All substrates were purchased from Bachem. Enzymatic reactions were monitored with five different inhibitor concentrations for 60 min in duplicate measurements. Time-dependent product formation was analyzed via non-linear regression using the equation [P] = v<sub>i</sub> × (1 - exp(-k<sub>obs</sub> × t)/k<sub>obs</sub>) + d, where [P] is the product concentration, v<sub>i</sub> the initial product formation rate, k<sub>obs</sub> the observed pseudo-first order rate constant, and d the offset. Values for k<sub>obs</sub> were plotted versus inhibitor concentrations, and second-order rate constants of inactivation k<sub>inac</sub>/K<sub>i</sub> were determined by non-linear regression using the equation k<sub>obs</sub> = k<sub>inac</sub> × [I]/(K<sub>i</sub> × (1 + [S]/K<sub>m</sub>) + [I]), where k<sub>inac</sub> is the first-order rate constant of irreversible inhibition, [I] the inhibitor concentration, K<sub>i</sub> the dissociation constant of the non-covalent enzyme-inhibitor complex, [S] the substrate concentration, and K<sub>m</sub> the Michaelis-Menten constant. Deviation of each data point from the calculated non-linear regression was less than 10%.

**Rhodesain inhibition assay:** Heterologously expressed and purified rhodesain was dissolved in 10 mM sodium citrate buffer pH 5.0 to a concentration of 4 mg/mL, diluted 1:850 with activation buffer (50 mM sodium acetate pH 5.5, 200 mM NaCl, 5 mM EDTA, 2 mM DTT), incubated at 37 °C for 30 min and then stored on ice. Prior to the measurements, this solution was further diluted 1:50 with activation buffer. A 2.5 mM solution of the substrate Z-Phe-Arg-AMC was prepared in DMSO. In 96-well plates, 195 μL assay buffer (50 mM sodium acetate buffer pH 5.5, 200 mM NaCl, 5 mM EDTA,

0.005% Brij 35) were mixed with 0.8 μL of the fluorogenic substrate, DMSO and/or inhibitor solution (3.2 μL). Upon addition of rhodesain (1 μL), the reaction was followed at 37 °C. The final enzyme concentration was 0.47 ng/mL, the final substrate concentration was 10 μM (= 13.05 × K<sub>m</sub>) and the total DMSO concentration was 2%. The K<sub>m</sub> value was determined in triplicate measurements with ten substrate concentrations (0.2–20 μM).

**Preparation of HEK cell lysate:** Human embryonic kidney (HEK) 293 cells were cultivated at 37 °C in Dulbecco's Modified Eagle's Medium (DMEM) containing fetal bovine serum (FBS) and penicillin/streptomycin (each 100 mg/mL). When a confluence of approximately 70% was reached, the culture medium was discarded, and the cells were washed twice with phosphate buffered saline (PBS). After further incubation at 37 °C in Minimal Essential Medium (Opti-MEM), the supernatant was discarded and the cells were mechanically lysed in PBS through a syringe. After brief centrifugation at 2000 g and 4 °C, the supernatant was collected, the protein concentration was determined using Roti-Nanoquant Bradford solution (Roth) and subsequently stored at –20 °C.

**Cultivation of *T. b. brucei* and *T. b. gambiense* and preparation of cell lysates:** The bloodstream forms of *T. b. brucei* Lister 427 and *T. b. gambiense* LiTAT 1.3 were cultivated in HMI-11 medium and 10% FBS at 37 °C in a humidified atmosphere of 5% CO<sub>2</sub>.<sup>[30]</sup> Total of 9 × 10<sup>7</sup> cells (10 mL) were collected by centrifugation and washed with PBS. Soluble protein extracts (0.8 mg protein/mL) were prepared by homogenization of the harvested cells in 100 mM sodium acetate buffer pH 5.5, 1 mM EDTA, 1% CHAPS on ice. The lysates were cleared by centrifugation (16,000 g, 10 min, 4 °C), filtered with Ultrafree-MC 0.22 μm (Millipore), and stored at –80 °C.

**SDS-PAGE analysis, in-gel and on-blot detection of rhodesain with probes 6 and 7:** *General.* A stock solution of recombinant rhodesain at a concentration of 2.5 mg/mL in 100 mM sodium acetate buffer pH 5.5 containing 150 mM NaCl was used and appropriately diluted. Stock solutions of E-64 (2 mM), K11777 (2 mM), ABPs 6 (0.5 mM) and 7 (0.5 mM) were prepared in DMSO. All incubations were performed in a total volume of 13 μL in assay buffer (100 mM sodium acetate buffer pH 5.5, 1 mM EDTA, 2.5 mM DTT) with an ABP concentration of 5 μM and a DMSO concentration of 2%. The reactions were stopped by addition of 7 μL of 4 × Bolt LDS Sample buffer with 500 mM DTT as reducing agent (Invitrogen) and heating at 75 °C for 10 min. The proteins were separated on 4–12% bis-tris polyacrylamide gels with MES running buffer (Bolt series from Invitrogen) alongside a pre-stained protein ladder (Thermo Fisher Scientific). For in-gel detection, the gels were visualized by a Typhoon RGB imager (GE Healthcare Life Sciences) using excitation at 488 nm and the Cy2 emission filter (λ<sub>em</sub> = 525 nm, band pass 20 nm) and subsequently stained with Coomassie Brilliant Blue (CBB). For on-blot detection, the proteins after SDS-PAGE separation were transferred from the gel to a PVDF membrane at 100 V for 60 min in transfer buffer (25 mM Tris/HCl pH 8.3, 190 mM glycine, 20% MeOH). Blots were visualized by using a chemiluminescent biotin-streptavidin detection system as follows. The membrane was blocked with 5% BSA in 50 mM Tris/HCl pH 7.6, 150 mM NaCl, 0.1% Tween 20 (TTBS) for 60 min, washed with TTBS, incubated for 60 min with streptavidin-horseradish peroxidase (HRP) conjugate (Sigma Aldrich; diluted 1:2500 in TTBS), washed with TTBS, and developed with the Immobilon Forte Western HRP substrate (Merck Millipore). Visualization was performed with an ImageQuant LAS 4000 mini CCD camera (GE Healthcare Life Sciences). In parallel, a separate membrane with identical samples was stained with Coomassie Brilliant Blue. *Competition assay.* To 5 μL of a rhodesain solution (0.25 mg/mL in 100 mM sodium acetate buffer pH 5.5, 150 mM NaCl), 5 μL of a solution containing E-64 and K11777 (20 μM each in assay buffer) was added. The mixture was incubated at 37 °C for 15 min. Next, 3 μL of a solution

of ABP 6 (21.7  $\mu\text{M}$  in assay buffer) was added and it was incubated at 25  $^{\circ}\text{C}$  for 60 min. In parallel, 5  $\mu\text{L}$  of the rhodesain solution, 5  $\mu\text{L}$  of assay buffer, and 3  $\mu\text{L}$  of the solution of ABP 6 (21.7  $\mu\text{M}$  in assay buffer) were incubated at 25  $^{\circ}\text{C}$  for 60 min. Likewise, ABP 7 was used in the competition experiment. SDS-PAGE analysis, in-gel and on-blot detection of rhodesain (1.25  $\mu\text{g}$ ) were performed as described above. *Estimation of the detection limit of probes 6 and 7.* Rhodesain (0.001–1  $\mu\text{g}$ ) was incubated with ABP 6 or 7 (final concentration: 5  $\mu\text{M}$ ) at 25  $^{\circ}\text{C}$  for 60 min, and SDS-PAGE analysis, in-gel and on-blot detection of rhodesain were performed as described above. *HEK cell lysate spiking.* Rhodesain (1.25  $\mu\text{g}$ ) was incubated with HEK cell lysate (30  $\mu\text{g}$  protein) and ABP 7 (final concentration: 5  $\mu\text{M}$ ) at 25  $^{\circ}\text{C}$  for 60 min. In control experiments, rhodesain or HEK cell lysate, or HEK cell lysate pretreated with a mixture of the competitive inhibitors E-64 and K11777 (10  $\mu\text{M}$  each) were separately treated with ABP 7 (final concentration: 5  $\mu\text{M}$ ). SDS-PAGE analysis, in-gel and on-blot detection of rhodesain were performed as described above.

**Imaging of rhodesain-type proteases in *Trypanosoma* cell lysates:** Soluble protein extracts of *T. b. brucei* and *T. b. gambiense* cells (5–100  $\mu\text{g}$  protein) were incubated at 25  $^{\circ}\text{C}$  with 5  $\mu\text{M}$  ABP 7 in 100 mM sodium acetate buffer pH 5.5, 1 mM EDTA, 2.5 mM DTT for 60 min. Competition assay was performed after preincubation of lysates with a mixture of the competitive inhibitors E-64 and K11777 (10  $\mu\text{M}$  each), or with inhibitor 1 or 2 (0.016–10  $\mu\text{M}$ ) for 30 min. The labeled proteins were acetone precipitated, resolved by SDS-PAGE, and visualized as described above.

**SE-HPLC-based detection of rhodesain with probes 6 and 7:** *General.* A stock solution of recombinant rhodesain at a concentration of 2.5 mg/mL in 100 mM sodium acetate buffer pH 5.5 containing 150 mM NaCl was used and appropriately diluted. All incubations were performed in a total volume of 20  $\mu\text{L}$  in assay buffer (100 mM sodium acetate buffer pH 5.5, 1 mM EDTA, 2.5 mM DTT) with a probe concentration of 15  $\mu\text{M}$  and a DMSO concentration of 1.6%. For reasons of enzyme stability, BSA (0.5  $\mu\text{g}$ ) was added to all incubations. Reactions were stopped by protein precipitation with 80% acetone. After 60 min incubation at 25  $^{\circ}\text{C}$ , the samples were centrifuged at 12,000 g at 4  $^{\circ}\text{C}$  for 15 min, the supernatants were carefully removed and the pellets were dried in a Maxi VacScan speed centrifuge coupled to a Scanvac CoolSafe freeze dryer (Labogene) at 40  $^{\circ}\text{C}$  and 200 rpm for 25 min and resuspended in 25  $\mu\text{L}$  of 100 mM sodium acetate buffer pH 5.5. Volumes of 20  $\mu\text{L}$  were injected into a Jasco 2000 HPLC system equipped with a TSKgel G2000SWXL size-exclusion (SE) column (7.8 mm I.D., 30 cm length, 5  $\mu\text{m}$  particle size, Tosoh), a DG-2080-53 degasser, a LG-2080-025 low pressure gradient unit, a PU-2080 Plus pump, a Rheodyne 8125 low dispersion injector with a 20  $\mu\text{L}$  injection loop, a CO-2060 column oven, a UV-2075 detector, and a FP-2020 fluorescence detector. Parallel detection was performed using the UV detector (280 nm) and the fluorescence detector ( $\lambda_{\text{ex}} = 426$  nm,  $\lambda_{\text{em}} = 470$  nm; gain = 10). The column oven temperature was set to 25  $^{\circ}\text{C}$ . The mobile phase consisted of 100 mM sodium phosphate buffer pH 6.7, 100 mM  $\text{Na}_2\text{SO}_4$ , and 0.05%  $\text{NaN}_3$ . The flow rate was 1 mL/min. ChromPass software (version 1.8.6.1) was used for HPLC system control and data analysis. *Quantification of rhodesain with probes 6 and 7.* Rhodesain solutions of different concentrations were incubated with ABP 6 or 7 (final concentration: 15  $\mu\text{M}$ ) at 25  $^{\circ}\text{C}$  for 60 min. The HPLC-based detection of rhodesain was performed as noted above. The final rhodesain concentrations were 10  $\mu\text{g}/\text{mL}$ , 20  $\mu\text{g}/\text{mL}$ , 40  $\mu\text{g}/\text{mL}$ , 60  $\mu\text{g}/\text{mL}$ , and 80  $\mu\text{g}/\text{mL}$ . The experiment was performed in triplicate. The mean areas under the curve (AUCs) of chromatograms resulting from fluorescence detection were plotted versus the rhodesain concentrations and analyzed using GraphPad Prism 8. *Competition assay.* To 5  $\mu\text{L}$  of a rhodesain solution (0.5 mg/mL in 100 mM sodium acetate buffer

pH 5.5 containing 150 mM NaCl), 10  $\mu\text{L}$  of a solution of E-64 (22.5  $\mu\text{M}$  in assay buffer) was added. The mixture was incubated at 37  $^{\circ}\text{C}$  for 15 min. Next, 5  $\mu\text{L}$  of a solution of ABP 6 (60  $\mu\text{M}$  in assay buffer) was added and it was incubated at 25  $^{\circ}\text{C}$  for 60 min. In parallel, 5  $\mu\text{L}$  of the rhodesain solution, 10  $\mu\text{L}$  of assay buffer, and 5  $\mu\text{L}$  of the solution of ABP 6 were incubated at 25  $^{\circ}\text{C}$  for 60 min. Likewise, ABP 7 was used in the competition experiment. SE-HPLC-based detection of rhodesain (2  $\mu\text{g}$ ) was performed as described above. *HEK cell lysate spiking.* Rhodesain (2.5  $\mu\text{g}$ ) was incubated with HEK cell lysate (45  $\mu\text{g}$  protein) and ABP 6 (final concentration: 15  $\mu\text{M}$ ) at 25  $^{\circ}\text{C}$  for 60 min. In parallel, rhodesain or HEK cell lysate were separately treated with ABP 6 (final concentration: 15  $\mu\text{M}$ ). Likewise, ABP 7 was used in the HEK cell lysate spiking experiment. The HPLC-based detection of rhodesain (2  $\mu\text{g}$ ) was performed as described above. *Streptavidin-based affinity chromatography.* Rhodesain solutions (2.5 mg/mL in 100 mM sodium acetate buffer pH 5.5, 150 mM NaCl) were used and appropriately diluted. Incubations were performed with a total amount of 2  $\mu\text{g}$  rhodesain. Incubations and protein precipitation were carried out as noted above. The pellets were resuspended in 100  $\mu\text{L}$  of buffer W (100 mM Tris/HCl buffer pH 8.0, 150 mM NaCl, 1 mM EDTA) and loaded onto a Strep-Tactin XT column (bed volume 0.2 mL; IBA). The column was washed with 5  $\times$  200  $\mu\text{L}$  of buffer W, fractions of 200  $\mu\text{L}$  were collected, and fractions 2–4 were pooled. Column-bound protein was eluted with 600  $\mu\text{L}$  of buffer E (100 mM Tris/HCl pH 8.0, 150 mM NaCl, 1 mM EDTA, 50 mM D-(+)-biotin). Wash and elution fractions were each concentrated to approximately 60  $\mu\text{L}$  with Amicon centrifugal filter units (Millipore; 4 mL; 10 kDa cut-off) by centrifugation at 7,500 g and 4  $^{\circ}\text{C}$ . For buffer exchange, 600  $\mu\text{L}$  buffer W was added and fractions were further centrifuged until a volume of approximately 60  $\mu\text{L}$  was reached. Aliquots (20  $\mu\text{L}$ ) were used for HPLC analysis.

## Acknowledgements

C.L. was supported by a fellowship from the BIGS DrugS graduate school of the University of Bonn. D.F. was supported by the German Academic Scholarship Foundation (Studienstiftung des deutschen Volkes). A.J., M.M. and M.H. were supported by the project ChemBioDrug CZ.02.1.01/0.0/0.0/16\_019/0000729 from ERDF/OPRDE and the institutional project RVO 61388963. A.Z. was supported by the Czech Ministry of Education grant OPVVV16\_019/0000759. The authors thank Antonia Leonhardt, Henry Anders, Beate Dik, Anna Odvárková, Marion Schneider, Sabine Terhart-Krabbe, Dr. Matthias D. Mertens, and Martina Slapničková for support and James T. Palmer and William R. Roush for providing inhibitors (K11002, K11017, WRR200, WRR255, WRR483). Open Access funding enabled and organized by Projekt DEAL.

## Conflict of Interest

The authors declare no conflict of interest.

## Data Availability Statement

The data that support the findings of this study are available from the corresponding author upon reasonable request.

**Keywords:** activity-based probes · affinity chromatography · cysteine proteases · imaging agents · peptidomimetics · rhodesain · size exclusion chromatography

- [1] a) A. Pogorzelska, B. Żolnowska, R. Bartoszewski, *Biochimie* **2018**, *151*, 85–106; b) A. Pišlar, A. Mitrovič, J. Sabotič, U. Pečar Fonovič, M. Perišič Nanut, T. Jakoš, E. Senjor, J. Kos, *PLoS Pathog.* **2020**, *16*, e1009013.
- [2] a) L. I. McCall, J. H. McKerrow, *Trends Parasitol.* **2014**, *30*, 342–349; b) R. Ettari, S. Previti, L. Tamborini, G. Cullia, S. Grasso, M. Zappalà, *Mini-Rev. Med. Chem.* **2016**, *16*, 1374–1391; c) J. L. Siqueira-Neto, A. Debnath, L. I. McCall, J. A. Bernatchez, M. Ndao, S. L. Reed, P. J. Rosenthal, *PLoS Neglected Trop. Dis.* **2018**, *12*, e0006512.
- [3] P. Johé, E. Jaenicke, H. Neuweiler, T. Schirmeister, C. Kersten, U. A. Hellmich, *J. Biol. Chem.* **2021**, *296*, 100565.
- [4] C. R. Caffrey, E. Hansell, K. D. Lucas, L. S. Brinen, A. Alvarez Hernandez, J. Cheng, S. L. Gwaltney, W. R. Roush, Y. D. Stierhof, M. Bogyo, D. Steverding, J. H. McKerrow, *Mol. Biochem. Parasitol.* **2001**, *118*, 61–73.
- [5] D. Steverding, D. W. Sexton, X. Wang, S. S. Gehrke, G. K. Wagner, C. R. Caffrey, *Int. J. Parasitol.* **2012**, *42*, 481–488.
- [6] I. D. Kerr, P. Wu, R. Marion-Tsukamaki, Z. B. Mackey, L. S. Brinen, *PLoS Neglected Trop. Dis.* **2010**, *4*, e701.
- [7] P. Johé, S. Jung, E. Endres, C. Kersten, C. Zimmer, W. Ye, C. Sönnichsen, U. A. Hellmich, C. Sotriffer, T. Schirmeister, H. Neuweiler, *ACS Chem. Biol.* **2021**, *16*, 661–670.
- [8] a) T. Schirmeister, J. Schmitz, S. Jung, T. Schmenger, R. L. Krauth-Siegel, M. Gütschow, *Bioorg. Med. Chem. Lett.* **2017**, *27*, 45–50; b) L. Cianni, C. Lemke, E. Gilberg, C. Feldmann, F. Rosini, F. dos Reis Rocho, J. F. Ribeiro, D. Y. Tezuka, C. D. Lopes, S. de Albuquerque, J. Bajorath, S. Laufer, A. Leitão, M. Gütschow, C. A. Montanari, *PLoS Neglected Trop. Dis.* **2020**, *14*, e0007755.
- [9] M. Giroud, B. Kuhn, S. Saint-Auret, C. Kuratli, R. E. Martin, F. Schuler, F. Diederich, M. Kaiser, R. Brun, T. Schirmeister, W. Haap, *J. Med. Chem.* **2018**, *61*, 3370–3388.
- [10] S. Previti, R. Ettari, S. Cosconati, G. Amendola, K. Chouchene, A. Wagner, U. A. Hellmich, K. Ulrich, R. L. Krauth-Siegel, P. R. Wich, I. Schmid, T. Schirmeister, J. Gut, P. J. Rosenthal, S. Grasso, M. Zappalà, *J. Med. Chem.* **2017**, *60*, 6911–6923.
- [11] a) R. Ettari, S. Previti, S. Maiorana, G. Amendola, A. Wagner, S. Cosconati, T. Schirmeister, U. A. Hellmich, M. Zappalà, *J. Med. Chem.* **2019**, *62*, 10617–10629; b) S. Maiorana, R. Ettari, S. Previti, G. Amendola, A. Wagner, S. Cosconati, U. A. Hellmich, T. Schirmeister, M. Zappalà, *ChemMedChem* **2020**, *15*, 1552–1561.
- [12] a) E. Dunny, W. Doherty, P. Evans, J. P. G. Malthouse, D. Nolan, A. J. S. Knox, *J. Med. Chem.* **2013**, *56*, 6638–6650; b) H. Zhang, J. Collins, R. Nyamwihura, S. Ware, M. Kaiser, I. V. Ogungbe, *Bioorg. Med. Chem. Lett.* **2018**, *28*, 1647–1651.
- [13] H. Zhang, J. Collins, R. Nyamwihura, O. Crown, O. Ajayi, I. V. Ogungbe, *Bioorg. Med. Chem. Lett.* **2020**, *30*, 127217.
- [14] A. Breuning, B. Degel, F. Schulz, C. Büchold, M. Stempka, U. Machon, S. Heppner, C. Gelhaus, M. Leippe, M. Leyh, C. Kisker, J. Rath, A. Stich, J. Gut, P. J. Rosenthal, C. Schmuck, T. Schirmeister, *J. Med. Chem.* **2010**, *53*, 1951–1963.
- [15] K. Arafet, F. V. González, V. Moliner, *Chem. Eur. J.* **2021**, *27*, 10142–10150.
- [16] I. D. Kerr, J. H. Lee, C. J. Farady, R. Marion, M. Rickert, M. Sajid, K. C. Pandey, C. R. Caffrey, J. Legac, E. Hansell, J. H. McKerrow, C. S. Craik, P. J. Rosenthal, L. S. Brinen, *J. Biol. Chem.* **2009**, *284*, 25697–25703.
- [17] For a recent review, see H. Fang, B. Peng, S. Y. Ong, Q. Wu, L. Li, S. Q. Yao, *Chem. Sci.* **2021**, *12*, 8288–8310.
- [18] For examples, see a) Z. Na, L. Li, M. Uttamchandani, S. Q. Yao, *Chem. Commun.* **2012**, *48*, 7304–7306; b) M. Frizler, I. V. Yampolsky, M. S. Baranov, M. Stirnberg, M. Gütschow, *Org. Biomol. Chem.* **2013**, *11*, 5913–5921; c) L. E. Sanman, W. A. van der Linden, M. Verdoes, M. Bogyo, *Cell Chem. Biol.* **2016**, *23*, 793–804; d) C. M. Pichler, J. Krysiak, R. Breinbauer, *Bioorg. Med. Chem.* **2016**, *24*, 3291–3303; e) D. Dana, J. Garcia, A. I. Bhuiyan, P. Rathod, L. Joo, D. A. Novoa, S. Paroly, K. R. Fath, E. J. Chang, S. K. Pathak, *Bioorg. Chem.* **2019**, *85*, 505–514; f) M. A. T. van de Plassche, T. J. O'Neill, T. Seeholzer, B. Turk, D. Krappmann, S. H. L. Verhelst, *J. Med. Chem.* **2020**, *63*, 3996–4004; g) C. Lemke, J. Benýšek, D. Brajtenbach, C. Breuer, A. Jilková, M. Horn, M. Buša, L. Ulrychová, A. Illies, K. F. Kubatzky, U. Bartz, M. Mareš, M. Gütschow, *J. Med. Chem.* **2021**, *64*, 13793–13806; h) A. I. Bhuiyan, P. Rathod, S. Ghoshal, D. Dana, T. Das, G. Li, A. A. Dickson, F. Rafi, G. S. Subramaniam, K. R. Fath, S. Paroly, E. J. Chang, S. K. Pathak, *Bioorg. Chem.* **2021**, *117*, 105463.
- [19] a) I. Florent, F. Lecaillon, J. J. Montagne, F. Gauthier, J. Schrével, G. Lalmanach, *Biol. Chem.* **2005**, *386*, 401–406; b) E. Deu, M. J. Leyva, V. E. Albrow, M. J. Rice, J. A. Ellman, M. Bogyo, *Chem. Biol.* **2010**, *17*, 808–819; c) P. Y. Yang, M. Wang, L. Li, H. Wu, C. Y. He, S. Q. Yao, *Chem. Eur. J.* **2012**, *18*, 6528–6541.
- [20] a) S. Arastu-Kapur, E. L. Ponder, U. P. Fonovič, S. Yeoh, F. Yuan, M. Fonovič, M. Grainger, C. I. Phillips, J. C. Powers, M. Bogyo, *Nat. Chem. Biol.* **2008**, *4*, 203–213; b) P. Y. Yang, M. Wang, C. Y. He, S. Q. Yao, *Chem. Commun.* **2012**, *48*, 835–837; c) J. W. Choy, C. Bryant, C. M. Calvet, P. S. Doyle, S. S. Gunatilleke, S. S. F. Leung, K. K. H. Ang, S. Chen, J. Gut, J. A. Osés-Prieto, J. B. Johnston, M. R. Arkin, A. L. Burlingame, J. Taunton, M. P. Jacobson, J. M. McKerrow, L. M. Podust, A. R. Renslo, *Beilstein J. Org. Chem.* **2013**, *9*, 15–25; d) M. S. Y. Tan, D. Davison, M. I. Sanchez, B. M. Anderson, S. Howell, A. Snijders, L. E. Edgington-Mitchell, E. Deu, *PLoS One* **2020**, e0227341.
- [21] For examples, see a) P. C. Trippier, *ChemMedChem* **2013**, *8*, 190–201; b) S. Chakrabarty, J. P. Kahler, M. A. van de Plassche, R. Vanhoutte, S. H. L. Verhelst, *Curr. Top. Microbiol. Immunol.* **2019**, *420*, 253–281; c) H. A. Beard, D. Korovesis, S. Chen, S. H. L. Verhelst, *Mol. Omics* **2021**, *17*, 197–209.
- [22] a) P. Jaishankar, E. Hansell, D. M. Zhao, P. S. Doyle, J. H. McKerrow, A. R. Renslo, *Bioorg. Med. Chem. Lett.* **2008**, *18*, 624–628; b) S. Jung, N. Fuchs, P. Johe, A. Wagner, E. Diehl, T. Yuliani, C. Zimmer, F. Barthels, R. A. Zimmermann, P. Klein, W. Waigel, J. Meyer, T. Opatz, S. Tenzer, U. Distler, H. J. Räder, C. Kersten, B. Engels, U. A. Hellmich, J. Klein, T. Schirmeister, *J. Med. Chem.* **2021**, *64*, 12322–12358.
- [23] J. Breidenbach, U. Bartz, M. Gütschow, *Biochim. Biophys. Acta Proteins Proteom.* **2020**, *1868*, 140445.
- [24] G. Kada, H. Falk, H. J. Gruber, *Biochim. Biophys. Acta* **1999**, *1427*, 33–43.
- [25] D. Steverding, C. R. Caffrey, *Mol. Biochem. Parasitol.* **2021**, *245*, 111395.
- [26] a) J. T. Palmer, D. Rasnick, J. L. Klaus, D. Brömme, *J. Med. Chem.* **1995**, *38*, 3193–3196; b) W. R. Roush, S. L. Gwaltney, J. Cheng, K. A. Scheidt, J. H. McKerrow, E. Hansell, *J. Am. Chem. Soc.* **1998**, *120*, 10994–10995; c) Y. T. Chen, L. S. Brinen, I. D. Kerr, E. Hansell, P. S. Doyle, J. H. McKerrow, W. R. Roush, *PLoS Neglected Trop. Dis.* **2010**, *4*, e825.
- [27] D. Häußler, A. C. Schulz-Fincke, A. M. Beckmann, A. Keils, E. Gilberg, M. Mangold, J. Bajorath, M. Stirnberg, T. Steinmetzer, M. Gütschow, *Chem. Eur. J.* **2017**, *23*, 5205–5209.
- [28] M. Frizler, F. Lohr, M. Lülsdorff, M. Gütschow, *Chem. Eur. J.* **2011**, *17*, 11419–11423.
- [29] M. D. Mertens, J. Schmitz, M. Horn, N. Furtmann, J. Bajorath, M. Mareš, M. Gütschow, *ChemBioChem* **2014**, *15*, 955–959.
- [30] H. Hirumi, K. Hirumi, *J. Parasitol.* **1989**, *75*, 985–989.

Manuscript received: May 26, 2022

Accepted manuscript online: July 19, 2022

Version of record online: September 7, 2022